Mechanism of Rapid Electron Transfer during Oxygen Activation in the R2 Subunit of *Escherichia coli* Ribonucleotide Reductase. 1. Evidence for a Transient Tryptophan Radical

Jeffrey Baldwin,[§] Carsten Krebs,[†] Brenda A. Ley,[§] Dale E. Edmondson,[‡] Boi Hanh Huynh,[†] and J. Martin Bollinger, Jr.*,[§]

Contribution from the Department of Biochemistry and Molecular Biology, The Pennsylvania State University, University Park, Pennsylvania 16802, and the Departments of Biochemistry, Chemistry, and Physics, Emory University, Atlanta, Georgia 30322

Received April 12, 2000

Abstract: Activation of dioxygen at the carboxylate-bridged diiron(II) cluster in the R2 subunit of *Escherichia coli* class I ribonucleotide reductase produces the enzyme's catalytically essential stable tyrosyl radical by one-electron oxidation of tyrosine 122. An intermediate in the reaction, the formally Fe(IV)Fe(III) cluster **X**, can oxidize Y122 in the final and rate-limiting step. During formation of **X**, an "extra" electron must be transferred to an as-yet-uncharacterized adduct between O_2 and the diiron(II) cluster. It was previously shown that a transient, broad absorption band centered near 560 nm develops when the reaction is carried out without an obvious exogenous source of the extra electron, and this band was ascribed to a tryptophan cation radical ($W^{+\bullet}$) resulting from temporary donation of the electron by the near-surface tryptophan residue 48 during formation of **X** [Bollinger, J. M., Jr.; Tong, W. H.; Ravi, N.; Huynh, B. H.; Edmondson, D. E.; Stubbe, J. *J. Am. Chem. Soc.* **1994**, *116*, 8024−8032]. In this work, we provide more definitive evidence for the $W^{+\bullet}$ assignment by showing that (1) the absorbing species reacts rapidly with reductants, (2) the species is associated with a $g = 2.0$ EPR signal and perturbs the EPR and Mössbauer spectra of **X**, and (3) most definitively, the absorption spectrum of the species from 310 to 650 nm closely matches the very distinctive spectrum of the tryptophan cation radical previously determined in pulse radiolysis studies [Solar, S.; Getoff, N.; Surdhar, P. S.; Armstrong, D. A.; Sing, A. *J. Phys. Chem.* **1991**, *95*, 3639−3643]. Quantitation of species at short reaction times by optical, EPR, and Mössbauer spectroscopies is consistent with the rapid formation of an intermediate containing both **X** and the $W^{+\bullet}$ (an **X**-$W^{+\bullet}$ diradical species). Formation of the $W^{+\bullet}$ (and presumably of **X**) is kinetically first order in both O_2 and Fe(II)-R2 complex, even at the highest reactant concentrations examined, which give a formation rate constant approaching 200 s^{-1}. This observation implies that precursors to the diradical species must not accumulate to greater than ∼10% of the initial Fe(II)-R2 reactant concentration and that the immediate precursor must generate the highly oxidizing $W^{+\bullet}$ with a rate constant of at least 400 s^{-1} at 5 °C.

Reductive activation of molecular oxygen by a carboxylate-bridged diiron(II) cluster is the *modus operandi* defining a class of proteins that includes the R2 subunit of class I ribonucleotide reductase[1] (hereafter simply R2[2]); bacterial hydrocarbon hydroxylases, such as methane monooxygenase hydroxylase (MMOH),[3−7] toluene-4-monooxygenase,[8] and alkane-ω-3 hydroxylase;[9,10] and plant fatty acyl desaturases, such as stearoyl acyl carrier protein Δ^9 desaturase (Δ9D).[11,12] Among the structurally characterized members of this class (the R2 proteins from *E. coli*[13−15] and mouse,[16] the MMOHs from *M. trichosporium*[17] and *M. capsulatus*,[7,18] and Δ9D from castor seed[19]), the protein folds defining the diiron sites and the structures of the diiron clusters themselves are remarkably similar.[20,21] Despite this similarity, the outcomes of their O_2 reactions are chemically diverse: O_2 activation in R2 leads to one-electron oxidation of

* To whom correspondence should be addressed.
§ Department of Biochemistry and Molecular Biology, Penn State University.
† Department of Physics, Emory University.
‡ Departments of Biochemistry and Chemistry, Emory University.

(1) Atkin, C. L.; Thelander, L.; Reichard, P.; Lang, G. *J. Biol. Chem.* **1973**, *248*, 7464−7472.

(2) Abbreviations used: R2, R2 subunit of ribonucleotide reductase; MMOH, hydroxylase component of methane monooxygenase; Δ9D, stearoyl acyl carrier protein Δ^9-desaturase; RNR, ribonucleotide reductase; $W^{+\bullet}$, tryptophan cation radical; Y122•, neutral tyrosyl radical derived from tyrosine number 122; **X**, the formally Fe(III)Fe(IV) cluster that accumulates during oxygen activation by R2; **X**-$W^{+\bullet}$, diradical species containing both **X** and the $W^{+\bullet}$; **X**-Y•, diradical species containing both **X** and Y122•; equiv, equivalents.

(3) Dalton, H. *Adv. Appl. Microbiol.* **1980**, *26*, 71−87.

(4) Woodland, M. P.; Patil, D. S.; Cammack, R.; Dalton, H. *Biochim. Biophys. Acta* **1986**, *873*, 237−242.

(5) Fox, B. G.; Surerus, K. K.; Münck, E.; Lipscomb, J. D. *J. Biol. Chem.* **1988**, *263*, 10553−10556.

(6) Fox, B. G.; Froland, W. A.; Dege, J. E.; Lipscomb, J. D. *J. Biol. Chem.* **1989**, *264*, 10023−10033.

(7) Rosenzweig, A. C.; Frederick, C. A.; Lippard, S. J.; Nordlund, P. *Nature* **1993**, *366*, 537−543.

(8) Pikus, J. D.; Studts, J. M.; Achim, C.; Kaufmann, K. E.; Münck, E.; Steffan, R. J.; McClay, K. B. G. *Biochemistry* **1996**, *35*, 9106−9119.

(9) Shanklin, J.; Whittle, E.; Fox, B. G. *Biochemistry* **1994**, *33*, 12787−12794.

(10) Shanklin, J.; Achim, C.; Schmidt, H.; Fox, B. G.; Münck, E. *Proc. Natl. Acad. Soc. U.S.A.* **1997**, *94*, 2981−2986.

(11) Fox, B. G.; Shanklin, J.; Somerville, C.; Münck, E. *Proc. Natl. Acad. Soc. U.S.A.* **1993**, *90*, 2486-2490.

(12) Fox, B. G.; Shanklin, J.; Ai, J.; Loehr, T. M.; Sanders-Loehr, J. *Biochemistry* **1994**, *33*, 12776−12786.

(13) Nordlund, P.; Sjöberg, B.-M.; Eklund, H. *Nature* **1990**, *345*, 593−598.

(14) Nordlund, P.; Eklund, H. *J. Mol. Biol.* **1993**, *232*, 123−164.

(15) Logan, D. T.; Su, X.-D.; Åberg, A.; Regnström, K.; Hajdu, J.; Eklund, H.; Nordlund, P. *Structure* **1996**, *4*, 1053−1064.

10.1021/ja001278u CCC: $19.00
Published on Web 11/22/2000

Scheme 1

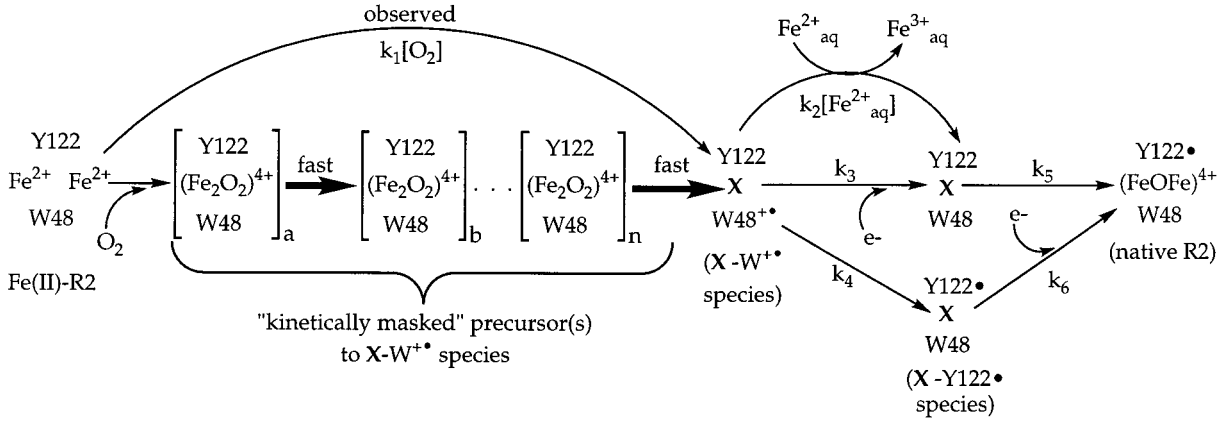

a tyrosine residue, generating the stable tyrosyl radical that is required for the catalytic activity of RNR,[1,22] while the O_2 reactions of the bacterial alkane hydroxylases and fatty acyl desaturase lead to distinct two-electron oxidations (hydroxylation and desaturation, respectively) of unactivated hydrocarbon substituents.[3,23]

A step that distinguishes the R2 reaction mechanism from those of the diiron hydroxylases and (presumably) desaturases is the transfer of a single exogenous electron to an intermediate formed upon or after addition of O_2 to the diiron(II) cluster.[24−29] As shown in Equation 1, this step balances the four-electron

$$2\text{Fe(II)} + \text{Y122} + \text{O}_2 + \text{H}^+ + \text{e}^- \rightarrow \text{Fe(III)-O}^{2-}\text{-Fe(III)} + \text{Y122}\bullet + \text{H}_2\text{O} \quad (1)$$

reduction of O_2 to the oxidation state of H_2O with the total of three electrons obtained by oxidation of the bound diiron(II) cluster and Y122. In the reaction of the best-studied of the R2 proteins, that from *E. coli*, the transfer of this electron (which has been called the "extra" electron[30,31]) is sufficiently rapid to have prevented characterization of intermediates that retain both oxidizing equivalents of the initial diiron(II)-O_2 complex.[27] Thus, whereas a peroxodiiron(III) complex (**P** or $\mathbf{H_{peroxo}}$) and a diiron(IV) complex (**Q**) have been shown to accumulate in sequence in the reaction of reduced MMOH with O_2 (in the presence of the effector protein, MMOB),[32−38] the only oxidized diiron intermediate to have been unambiguously demonstrated in the R2 reaction is the one-electron-oxidized (formally Fe(IV)Fe(III)) cluster **X** (Scheme 1).[24,25,27,39,40] On the basis of its characterization by Mössbauer,[40] EPR,[40,41] and ^{57}Fe ENDOR spectroscopies,[41] **X** has been formulated as an antiferromagnetically coupled Fe(IV)Fe(III) cluster with a total electron spin quantum number, S, of $^1/_2$ (explaining its free-radical-like $g = 2.0$ EPR signal).[41] ^{17}O and ^{1,2}H ENDOR studies have led to the proposal that it contains one μ-oxo ligand and one terminal hydroxo ligand on the Fe(III) ion.[42−44] The surprisingly short Fe−−Fe distance of 2.5 Å determined by EXAFS suggests the presence of two additional bridging ligands, which are likely to be μ-1,1- or μ-1,3-bridging carboxylates.[45] As it converts to the product μ-oxodiiron(III) cluster, **X** can oxidize Y122 to the radical.[24,25]

Two aspects of the R2 reaction that are still poorly understood are the mechanism of the electron-transfer step and the extent to which this step *solely* distinguishes the overall mechanism and outcome of O_2 activation in R2 from those of diiron hydroxylases and desaturases. With respect to the latter issue, most mechanistic proposals have invoked the *presumption* that the precursors to cluster **X** (the "kinetically-masked" $(Fe_2O_2)^{4+}$ species in Scheme 1) include structural homologues of MMOH **P** or **Q** or both. In this scenario, the electron-transfer step is

(16) Kauppi, B.; Nielsen, B. B.; Ramaswamy, S.; Kjøller-Larson, I.; Thelander, M.; Thelander, L.; Eklund, H. *J. Mol. Biol.* **1996**, *262*, 706−720.
(17) Elango, N.; Radhakrishnan, R.; Froland, W. A.; Waller, B. J.; Earhart, C. A.; Lipscomb, J. D.; Ohlendorf, D. H. *Protein Sci.* **1997**, *6*, 556−568.
(18) Rosenzweig, A. C.; Nordlund, P.; Takahara, P. M.; Frederick, C. A.; Lippard, S. J. *Chem. Biol.* **1995**, *2*, 409−418.
(19) Lindqvist, Y.; Huang, W.; Schneider, G.; Shanklin, J. *EMBO J.* **1996**, *15*, 4081−4092.
(20) Nordlund, P.; Eklund, H. *Curr. Opin. Struct. Biol.* **1995**, *5*, 758−766.
(21) Summa, C. M.; Lombardi, A.; Lewis, M.; DeGrado, W. F. *Curr. Opin. Struct. Biol.* **1999**, *9*, 500−508.
(22) Sjöberg, B.-M.; Reichard, P.; Gräslund, A.; Ehrenberg, A. *J. Biol. Chem.* **1977**, *252*, 536−541.
(23) Nagai, J.; Block, K. *J. Biol. Chem.* **1966**, *241*, 1925−1927.
(24) Bollinger, J. M., Jr.; Edmondson, D. E.; Huynh, B. H.; Filley, J.; Norton, J. R.; Stubbe, J. *Science* **1991**, *253*, 292−298.
(25) Bollinger, J. M., Jr.; Tong, W. H.; Ravi, N.; Huynh, B. H.; Edmondson, D. E.; Stubbe, J. *J. Am. Chem. Soc.* **1994**, *116*, 8015−8023.
(26) Bollinger, J. M., Jr.; Tong, W. H.; Ravi, N.; Huynh, B. H.; Edmondson, D. E.; Stubbe, J. *J. Am. Chem. Soc.* **1994**, *116*, 8024−8032.
(27) Tong, W. H.; Chen, S.; Lloyd, S. G.; Edmondson, D. E.; Huynh, B. H.; Stubbe, J. *J. Am. Chem. Soc.* **1996**, *118*, 2107−2108.
(28) Wallar, B. J.; Lipscomb, J. D. *Chem. Rev.* **1996**, *96*, 2625−2657.
(29) Solomon, E. I.; Brunold, T. C.; Davis, M. I.; Kemsley, J. N.; Lee, S.-K.; Lehnert, N.; Neese, F.; Skulan, A. J.; Yang, Y.-S.; Zhou, J. *Chem. Rev.* **2000**, *100*, 235−349.
(30) Bollinger, J. M., Jr.; Krebs, C.; Vicol, A.; Chen, S.; Ley, B. A.; Edmondson, D. E.; Huynh, B. H. *J. Am. Chem. Soc.* **1998**, *120*, 1094−1095.
(31) Miller, M. A.; Gobena, F. T.; Kauffmann, K.; Münck, E.; Que, L., Jr.; Stankovich, M. T. *J. Am. Chem. Soc.* **1999**, *121*, 1096−1097.
(32) Lee, S.-K.; Nesheim, J. C.; Lipscomb, J. D. *J. Biol. Chem.* **1993**, *268*, 21569−21577.
(33) Lee, S.-K.; Fox, B. G.; Froland, W. A.; Lipscomb, J. D.; Münck, E. *J. Am. Chem. Soc.* **1993**, *115*, 6450−6451.
(34) Liu, K. E.; Wang, D.; Huynh, B. H.; Edmondson, D. E.; Salifoglou, A.; Lippard, S. J. *J. Am. Chem. Soc.* **1994**, *116*, 7465−7466.
(35) Liu, K. E.; Valentine, A. M.; Wang, D.; Huynh, B. H.; Edmondson, D. E.; Salifoglou, A.; Lippard, S. J. *J. Am. Chem. Soc.* **1995**, *117*, 10174−10185.
(36) Shu, L. J.; Nesheim, J. C.; Kauffmann, K.; Münck, E.; Lipscomb, J. D.; Que, L., Jr. *Science* **1997**, *275*, 515−518.
(37) Valentine, A. M.; Stahl, S. S.; Lippard, S. J. *J. Am. Chem. Soc.* **1999**, *121*, 3876−3887.
(38) Lee, S.-K.; Lipscomb, J. D. *Biochemistry* **1999**, *38*, 4423−4432.
(39) Bollinger, J. M., Jr.; Stubbe, J.; Huynh, B. H.; Edmondson, D. E. *J. Am. Chem. Soc.* **1991**, *113*, 6289−6291.
(40) Ravi, N.; Bollinger, J. M., Jr.; Huynh, B. H.; Edmondson, D. E.; Stubbe, J. *J. Am. Chem. Soc.* **1994**, *116*, 8007−8014.
(41) Sturgeon, B. E.; Burdi, D.; Chen, S.; Huynh, B. H.; Edmondson, D. E.; Stubbe, J.; Hoffman, B. M. *J. Am. Chem. Soc.* **1996**, *118*, 7551−7557.
(42) Burdi, D.; Sturgeon, B. E.; Tong, W. H.; Stubbe, J.; Hoffman, B. M. *J. Am. Chem. Soc.* **1996**, *118*, 281−282.

envisaged to be primarily responsible for the divergence of the R2 and MMOH mechanisms and outcomes. The evidence for a peroxodiiron(III) complex in the R2 reaction[27] is, however, entirely equivocal, and no evidence whatsoever has been obtained for the intermediacy of a diiron(IV) complex. Consequently, it is also possible that O_2 activation in R2 follows a fundamentally different mechanism from that in MMOH and involves structurally distinct intermediates. In this scenario, the differences between the two proteins with respect to cluster coordination are envisaged to be important for directing formation of different intermediates with distinct reactivities.

With respect to the electron-transfer step, we and other investigators have proposed that it is mediated by a chain of hydrogen-bonded residues comprising a near-surface tryptophan (residue 48 in *E. coli* R2 and 103 in mouse R2), a second-sphere aspartate (237 and 266), and the histidine ligand to Fe1 of the cluster (118 and 173).[13,14,26,46−48] The precise mechanism of this step has, however, remained controversial. Although there is consensus that Fe(II) can donate the electron,[25,31,49,50] it is not yet clear whether the Fe(II) donor can be free in solution[51] or must be bound at the diiron cluster site of a different monomer[31,50] or at an additional site on the protein.[48] Moreover, whereas Schmidt et al. have characterized the electron-transfer step in mouse R2 as "transfer of a H• atom along a hydrogen-bonded chain" and have proposed that the H• atom originates from an $[Fe(H_2O)_6]^{2+}$ complex bound at the surface of the protein,[48] we have proposed that the cognate step in the *E. coli* R2 reaction proceeds by a shuttling mechanism involving transient one-electron oxidation of W48 and reduction of the resulting tryptophan cation radical (hereafter denoted $W^{+\bullet}$) by free Fe(II) or another reductant.[26] Our proposal was based on (1) the observations that a broad absorption band centered at 560 nm develops exclusively when no exogenous source of the extra electron is present in the reaction and that development and decay of this band are kinetically competent for the associated species to be on the pathway to formation of the tyrosyl radical,[24,26] (2) the similarity of this absorption band to the lower energy feature of indole cation radicals that have been generated by pulse radiolysis,[52,53] and (3) the previously noted similarity of the hydrogen-bonded chain involving W48 to one in cytochrome *c* peroxidase,[13,14,54] in which a $W^{+\bullet}$ is known to form from the cognate residue, W191, during catalytic reduction of hydrogen peroxide.[55−58] The failure of the transient absorption to develop in the R2 reaction in the presence of excess Fe(II) or ascorbate[25] was rationalized on the basis of the rapid reduction of the $W^{+\bullet}$ by these species.[26]

In this work we have more rigorously tested the W48-mediated electron-shuttling hypothesis by probing the chemical reactivity and spectroscopic characteristics of the 560-nm-absorbing species. Its reactivity toward reductants, its optical absorption spectrum from 310 to 650 nm (which we have resolved kinetically), its association with electron paramagnetic resonance absorption in the $g = 2.0$ region, and its magnetic coupling with cluster **X** are entirely consistent with the $W^{+\bullet}$ assignment. The kinetics of formation and decay of **X** and the $W^{+\bullet}$ at different concentrations of reactants (Fe(II)-R2 complex, O_2, free Fe(II) or other reductants) indicate that **X** and the $W^{+\bullet}$ are produced concomitantly, that the $W^{+\bullet}$ is an intermediate in the electron-transfer step even when a facile reductant is present to provide the electron, and that reduction of the $W^{+\bullet}$ by *free* Fe(II) and other reductants is very facile. The kinetic data also set a lower limit for the effective rate constant for decay of the precursors to the **X**-$W^{+\bullet}$ species. This limit is nearly 3 orders of magnitude greater than those for decay of characterized peroxodiiron(III) complexes such as MMOH **P**.

Materials and Methods

Preparation of Apo R2 and Fe(II)-R2 and Rapid-Freeze-Quench Experiments. The apparatus and procedures used to obtain and quantify apo R2 protein,[47] to prepare the Fe(II)-R2 complex in the absence of O_2,[47] to prepare freeze-quenched samples,[40] and to acquire EPR[39] and Mössbauer spectra[40] have been described elsewhere. Because minor modifications were implemented in several cases, additional details are provided in the Supporting Information. Specific attributes of each sample or experiment are given in the appropriate figure legend.

Stopped-Flow Spectrophotometry. Stopped-flow experiments were carried out on a KinTek Corporation Model SF-2001 stopped-flow spectrofluorimeter (path length 0.5 cm, deadtime 3 ms), which was equipped with a Gilford Model 240 light source and configured for sequential mixing. The apparatus was housed in an anoxic chamber (MBraun). The syringe(s) and flow-line(s) for the Fe(II)-R2 complex were soaked in 5 mM sodium dithionite solution for several hours and then washed scrupulously with dithionite-free, O_2-free buffer prior to loading of the stopped-flow apparatus. The temperature was maintained at 5 °C by a circulating water bath. Traces depicting the 411 nm peak height ($A_{411} - (A_{405} + A_{417})/2$), which is proportional to the concentration of tyrosyl radical,[25,51] were constructed from the averages of at least four trials at each individual wavelength. A_{560}-versus-time traces also represent the averages of at least four trials.

Kinetic Simulations. Kinetic simulations were carried out with the Microsoft Windows-based program KinTekSim (KinTek Corp., State College, PA). Kinetic data were analyzed according to Scheme 1, which is derived from the published mechanism shown and represents the minimal kinetic scheme necessary to accommodate all the data presented herein. The data that are simulated are of two types: absorbance at 560 nm versus time and 411 nm peak height ($A_{411} - (A_{405} + A_{417})/2$) versus time. In simulating the former traces, it was necessary to set the molar absorptivities at 560 nm (ϵ_{560}) for each species in Scheme 1. For the primary absorbing species, the $W^{+\bullet}$, the value of 3000 M^{-1} cm^{-1} determined in the pulse radiolysis studies of Solar et al.[52] was assumed. The methods by which values of ϵ_{560} were determined for the other species (which are minor contributors) are described in detail in the Supporting Information, and the values are compiled in Table 1.

(43) Willems, J.-P.; Lee, H.-I.; Burdi, D.; Doan, P. E.; Stubbe, J.; Hoffman, B. M. *J. Am. Chem. Soc.* **1997**, *119*, 9816−9824.
(44) Burdi, D.; Willems, J.-P.; Riggs-Gelasco, P.; Antholine, W. E.; Stubbe, J.; Hoffman, B. M. *J. Am. Chem. Soc.* **1998**, *120*, 12910−12919.
(45) Riggs-Gelasco, P. J.; Shu, L.; Chen, S.; Burdi, D.; Huynh, B. H.; Que, L., Jr.; Stubbe, J. *J. Am. Chem. Soc.* **1998**, *120*, 849−860.
(46) Rova, U.; Goodtzova, K.; Ingemarson, R.; Behravan, G.; Gräslund, A.; Thelander, L. *Biochemistry* **1995**, *34*, 4267−4275.
(47) Parkin, S. E.; Chen, S.; Ley, B. A.; Mangravite, L.; Edmondson, D. E.; Huynh, B. H.; Bollinger, J. M., Jr. *Biochemistry* **1998**, *37*, 1124−1130.
(48) Schmidt, P. P.; Rova, U.; Katterle, B.; Thelander, L.; Gräslund, A. *J. Biol. Chem.* **1998**, *273*, 21463-21472.
(49) Ochiai, E.; Mann, G. J.; Gräslund, A.; Thelander, L. *J. Biol. Chem.* **1990**, *265*, 15758−15761.
(50) Elgren, T. E.; Lynch, J. B.; Juarez-Garcia, C.; Münck, E.; Sjöberg, B.-M.; Que, L., Jr. *J. Biol. Chem.* **1991**, *266*, 19265−19268.
(51) Bollinger, J. M., Jr., 1993, Ph.D. Thesis, Massachusetts Institute of Technology.
(52) Solar, S.; Getoff, N.; Surdhar, P. S.; Armstrong, D. A.; Sing, A. *J. Phys. Chem.* **1991**, *95*, 3639−3643.
(53) Mishra, A. K.; Chandrasekar, R.; Faraggi, M.; Klapper, M. H. *J. Am. Chem. Soc.* **1994**, *116*, 1414−1422.
(54) Finzel, B. C.; Poulos, T. L.; Kraut, J. *J. Biol. Chem.* **1984**, *259*, 13027−13036.
(55) Sivaraja, M.; Goodin, D. B.; Smith, M.; Hoffman, B. M. *Science* **1989**, *245*, 738−740.
(56) Erman, J. E.; Vitello, L. B.; Mauro, J. M.; Kraut, J. *Biochemistry* **1989**, *28*, 7992−7995.
(57) Houseman, A. L. P.; Doan, P. E.; Goodin, D. B.; Hoffman, D. M. *Biochemistry* **1993**, *32*, 4430−4443.
(58) Huyett, J. E.; Doan, P. E.; Gurbiel, R.; Houseman, A. L.; Sivaraja, M.; Goodin, D. B.; Hoffman, B. M. *J. Am. Chem. Soc.* **1995**, *117*, 9033−9041.

Table 1. Molar Absorptivities Employed in the Kinetic Simulations

species	ϵ_{560} (M^{-1} cm^{-1})	$\epsilon_{411} - (\epsilon_{405} + \epsilon_{417})/2$ (M^{-1} cm^{-1})
Fe(II)-R2	0	0
$W^{+\bullet}$	3000	0
X	480	0
Fe^{3+}_{aq}	60	0
Y122$^\bullet$	180	1500
$(FeOFe)^{4+}$	200	0

For the case of the 411 nm peak height ($A_{411} - (A_{405} + A_{417})/2$) versus time traces, it was assumed that only the sharp feature of Y122$^\bullet$ contributes over this narrow 12-nm range. (The validity of this assumption has been demonstrated previously.[25]) It was further assumed that the presence of **X** adjacent to Y122$^\bullet$ does not alter the line shape of this feature and therefore that $\epsilon_{411} - (\epsilon_{405} + \epsilon_{417})/2$ of the **X**-Y$^\bullet$ diradical species is equal to $\epsilon_{411} - (\epsilon_{405} + \epsilon_{417})/2$ of native R2 (2150 $\pm$ 50 M^{-1} cm^{-1} on the Hewlett-Packard spectrophotometer). Due to the sharpness of the Y122$^\bullet$ absorption feature, $\epsilon_{411} - (\epsilon_{405} + \epsilon_{417})/2$ depends markedly on spectral resolution and wavelength calibration. Therefore, $\epsilon_{411} - (\epsilon_{405} + \epsilon_{417})/2$ of the tyrosyl radical in the stopped-flow apparatus was independently determined (1500 M^{-1} cm^{-1}) by comparing the amplitude of stopped-flow traces to [Y122$^\bullet$] determined by measuring (on the Hewlett-Packard spectrophotometer) the spectra of products recovered from the stopped-flow apparatus.

The remaining adjustable parameters in the simulations are the initial concentrations of O_2, reactive Fe(II)-R2 complex, and free Fe(II), and the rate constants k_1–k_6. The methods by which they were calculated or experimentally determined are described in detail in the Supporting Information, and the values for each simulation are compiled in Table 2. The degree to which each kinetic parameter is constrained by the experimental data is discussed in the Supporting Information.

Results and Discussion

Determination of Optimal Fe(II)/R2 Ratio. It was previously shown that the quantity of the 560-nm-absorbing species to accumulate (as reflected by the amplitude of the 560 nm transient) upon mixing apo R2 with Fe(II) in the presence of O_2 is exquisitely sensitive to the ratio of Fe(II)/R2.[26] As part of the present study, the ratio which gives the largest amplitude upon reaction of the preformed Fe(II)-R2 complex with O_2 was determined (Figure 1). The transient was found to have maximum amplitude ($A_{max} - A_{completion}$) with an Fe(II)/R2 ratio near 3.2 (inset to Figure 1). The complex dependence of the amplitude on Fe(II)/R2 ratio can be explained qualitatively as a result of two opposing factors. On one hand, rapid production of the intermediate requires that the protein have Fe(II) bound in dinuclear fashion. We previously showed that one of the two sites of the cluster (proposed to be site 2 in the nomenclature of Nordlund et al.[14]) has at least 5-fold greater affinity for (Fe(II)) than the other site.[59] As a result, complexation with low Fe(II)/R2 ratios gives primarily a mononuclear complex, which is unreactive to O_2. As the ratio is increased, the fractional occupancy of higher-affinity site increases, and the lower affinity site begins to fill to generate the reactive diiron(II) complex. Thus, the differential affinity explains the "induction" and "rise" phases of the inset to Figure 1 with Fe(II)/R2 values less than 3.2. On the other hand, it is shown below that free Fe(II) very efficiently reduces the 560-nm-absorbing species and limits its accumulation. In titration of our preparations of apo R2 with Fe(II) in the presence of O_2 and ascorbate, tyrosyl radical formation is complete after addition of 3.2 $\pm$ 0.1 equiv, and this equivalence point presumably represents the number of fully competent cluster-associated Fe(II) sites in the protein. Direct support for this interpretation comes from a recent study in which the anaerobic titration of apo R2 with Fe(II) was monitored by circular dichroism and magnetic circular dichroism spectroscopies.[60] In that study, development of the signature of the diiron(II) cluster was shown to saturate at this Fe(II)/R2 ratio, and features of $Fe(II)_{aq}$ became obvious at higher ratios. It is not clear why the protein possesses less than its theoretical complement of 4 sites per dimer, but preparations of R2 from different laboratories all exhibit this characteristic. Thus, as (Fe(II)/R2) surpasses 3.2, free Fe(II) becomes available to react with the 560-nm-absorbing species as it forms. This situation explains the sharp decrease in amplitude as Fe(II)/R2 increases above 3.2. In experiments to test for the proposed (**X**-$W^{+\bullet}$) diradical species by quantifying **X** by Mössbauer spectroscopy and total "spin" by EPR spectroscopy, it was desirable to maximize *both* the absolute concentration of the absorbing species and its concentration *relative to that of* ***X***. In this aim, the presence of free Fe(II) along with Fe(II)-R2 complex would represent a significant detriment, as it would lead to decay of the $W^{+\bullet}$ but not of **X**. If the lower affinity site were to have sufficiently high affinity to be in the tight-binding regime under the reaction conditions employed, an Fe(II)/R2 ratio of 3.2 would have been optimal. However, simulation of A_{560}-versus-time traces from experiments with varying Fe(II)/R2 (such as those in Figure 1) and experiments to probe Fe(II) binding directly have shown that the lower affinity site is *not* tight-binding at the R2 concentrations employed in this study. Therefore, an Fe(II)/R2 ratio of 3.0 was selected as the best compromise to maximize the concentration of the reactive Fe(II)-R2 complex while minimizing the concentration of free Fe(II). In other experiments, it was important only to minimize the concentration of free Fe(II), and ratios as low as 2.3 were employed.

Reactivity of the Intermediate toward Reductants. We previously inferred from the suppression of the 560-nm absorption by either excess Fe(II) or ascorbate that the intermediate is reduced rapidly by these species.[24,26] To test directly for this reactivity, Fe(II)-R2 (Fe/R2 = 2.3–3.0) was mixed with O_2-saturated buffer, the solution was allowed to age for sufficient time for the 560-nm-absorbing species to accumulate (0.016 s), and the intermediate was then mixed with reductant (ascorbate, additional Fe(II), or 2-mercaptoethanol). In the absence of a facile reductant, the intermediate has an intrinsic decay rate constant (the sum of k_3 and k_4 in Scheme 1) of 12.3 $\pm$ 2.5 s^{-1} (mean $\pm$ standard deviation from 31 independent determinations; data not shown) under the reaction conditions employed (see legend to Figure 2).[61] When the preformed intermediate is mixed with ascorbate at concentrations as low as 0.2 mM (with ascorbate in excess), decay of the 560-nm absorption is complete in the "deadtime" of the stopped-flow apparatus (~3 ms). The intermediate also reacts with additional Fe(II) (Figure 2A) and 2-mercaptoethanol (Figure 2B), and these reactions are kinetically first order in reductant, with second-order rate constants of 2.1 $\times$ 10^6 (inset to Figure 2A) and 4.0 $\times$ 10^4 M^{-1} s^{-1} (inset to Figure 2B), respectively. The acceleration of decay of the 560-nm-absorbing species by ascorbate, free Fe(II), and 2-mercaptoethanol indicates that the species is susceptible to reduction, as is expected for a $W^{+\bullet}$ at position 48. The observation of second-order kinetics implies a collisional reaction between the reductant (either $Fe(II)_{aq}$ or 2-mercaptoethanol) and the intermediate species, as opposed to mechanisms involving complex

(59) Bollinger, J. M., Jr.; Chen, S.; Parkin, S. E.; Mangravite, L. M.; Ley, B. A.; Edmondson, D. E.; Huynh, B. H. *J. Am. Chem. Soc.* **1997**, *119*, 5976–5977.

(60) Yang, Y.-S.; Baldwin, J.; Ley, B. A.; Bollinger, J. M., Jr.; Solomon, E. I. *J. Am. Chem. Soc.* **2000**, *122*, 8495–8510.

(61) The source of the electron to reduce the $W^{+\bullet}$ in the k_3-associated step is not known, but recent evidence suggests that the source might be the buffer (vide infra; J. Baldwin, B. Ley, J. Bollinger, unpublished data).

Table 2. Values of Reactant Concentrations and Rate Constants that Were Used To Generate the Simulated Traces Shown in Figures 8−11 According to Scheme 1[a]

figure	[Fe(II)-R2], mM	[O_2], mM	[$Fe(II)_{aq}$], mM	k_1, 10^5 M^{-1} s^{-1}	k_2, 10^5 M^{-1} s^{-1}	k_3, s^{-1}	k_4, s^{-1}	k_5, s^{-1}	k_6, s^{-1}
8	0.495	1.26	0.073	1.98	16	5.2	5.4	0.7	0.7
9A	0.0495	0.21 0.42 0.83	0	2.05	23	3.9	5.5	0.7	0.4
9B	0.11 0.22 0.43	0.051	0.007	2.20	23	6.7	7.3	0.7	0.7
10	0.071	0.83	0.11 0.23	2.10	21	4.0	6.0	0.9	0.5
11	0.20	0.83	0.014 0.34	2.5	18	5.0	5.0	0.97	0.5
mean and range				2.2 ± 0.3	21 ± 5	5.3 ± 1.4	6.2 ± 1.2	0.85 ± 0.15	0.59 ± 0.2

[a] The experimental conditions are given in the appropriate figure legend.

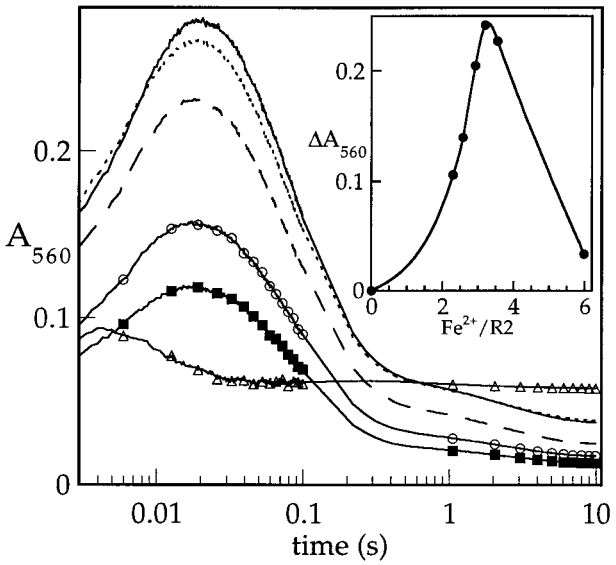

Figure 1. The dependence of the amplitude of the transient absorbance at 560 nm on the ratio Fe(II)/R2. Apo R2 was mixed in the absence of O_2 with Fe(II) in a molar ratio of 2.3 (filled squares), 2.6 (open circles), 2.9 (dashed line), 3.2 (solid line), 3.5 (dotted line), or 6.0 (open triangles). This solution was mixed in the stopped-flow apparatus at 5 °C in a 1:2 volume ratio with 100 mM Hepes, pH 7.6, which had been saturated at 24 °C with O_2. Due to the addition of slightly different volumes of the Fe(II) stock to the protein, the final concentration of R2 after mixing in the stopped-flow varied slightly from 0.18 mM for Fe(II)/R2 = 2.3 to 0.17 mM for Fe(II)/R2 = 6.0. The inset shows a plot of the maximum value of A_{560} minus the final value for each trace.

formation or a protein unimolecular isomerization prior to reduction. These observations seem inconsistent with the hypothesis of Que and co-workers that Fe(II) bound in the cluster site of one monomer is oxidized sacrificially to provide the electron for O_2 activation in another monomer.[31,50] The invariant and slow (12 s^{-1}) decay kinetics for the $W^{+\bullet}$ as the Fe(II)/R2 ratio changes from <2 to 3.2 and the contrasting rapid reduction by Fe(II) that is added after formation of the $W^{+\bullet}$ indicate that reduction by free Fe(II) is kinetically preferred to reduction by bound Fe(II). Moreover, the facile reduction by the thiol compound indicates that, even if the proposed intermonomer electron transfer can occur, it is unlikely to be physiologically significant.

Kinetic Resolution of the Absorption Spectrum of the Intermediate. The extremely distinctive absorption spectrum of indole cation radicals in the 310−650-nm region (small open squares and solid line in Figure 3) has been defined in several studies involving pulse radiolysis of dissolved indole derivatives, including tryptophan and tryptophan-containing peptides.[52,53] By exploiting the reactivity of the 560-nm-absorbing intermediate in R2 toward 2-mercaptoethanol, the full absorption spectrum of the intermediate from 310 to 650 nm was kinetically resolved for comparison to the known spectrum. The intermediate was preformed as before in the first stopped-flow mix, and the absorbance was followed as a function of time after the second mix with 2-mercaptoethanol (4 mM final concentration). A plot of the amplitude of decrease in absorbance between 4 and 14 ms after the second mix versus wavelength (open circles in Figure 3) agrees remarkably well with the known spectrum of the $W^{+\bullet}$,[52] including the sharp, intense feature at 335 nm that is obscured by absorption from **X** in standard stopped-flow monitoring of the R2 reaction. The amplitudes are consistent with the concentrations of reactants and the molar absorptivities determined by Solar et al.[52] The precise matching of *both* features of the $W^{+\bullet}$ spectrum by features from the R2 intermediate is much more compelling evidence for the assignment than the previously cited similarity of only the lower energy feature.

EPR and Mössbauer Evidence that the Absorbing Intermediate Is a Radical. A $W^{+\bullet}$ is expected to exhibit an EPR feature in the $g = 2.0$ region. To test if the 560-nm-absorbing species fulfills this criterion, samples for EPR characterization were prepared by mixing the Fe(II)-R2 complex (Fe(II)/R2 = 3.0) with O_2 and freeze-quenching at reaction times similar to those at which the absorbance at 560 nm reaches its maximum value (17 ± 1 ms under the reaction conditions employed; see Figure 8A). Samples quenched at 19 ms and 27 ms reaction times are distinctly purple, as expected for a species that absorbs at 560 nm. Samples quenched at reaction times exceeding 200 ms are not purple, as expected from the results of Figure 1. These observations confirm that the absorbing species can be successfully freeze-trapped. X-band EPR spectra at 20 K of the 19 and 27 ms samples prepared with ^{56}Fe exhibit a broad and featured signal at $g = 2.0$ (Figure 4, spectrum A), which is clearly different from the isotropic singlet of intermediate **X** (Figure 4, spectrum C). The spectra of samples prepared with ^{57}Fe (Figure 4, spectrum B) exhibit hyperfine broadening similar to that previously observed for **X**.[39] This observation suggests that some fraction of the rapidly developing $g = 2.0$ signal is contributed by **X**. This conclusion is verified by the presence of the paramagnetic signature of **X** in the Mössbauer spectra of a 19-ms sample prepared identically (Figure 5). A detailed analysis of the Mössbauer spectra, which is described below, indicates that 1.0 ± 0.1 equiv of **X**, 0.8 ± 0.1 equiv of unreacted Fe(II), and 0.12 ± 0.06 equiv of a paramagnetic high-spin ($S = {}^5/_2$) Fe(III) species are present in the sample. The EPR spectra

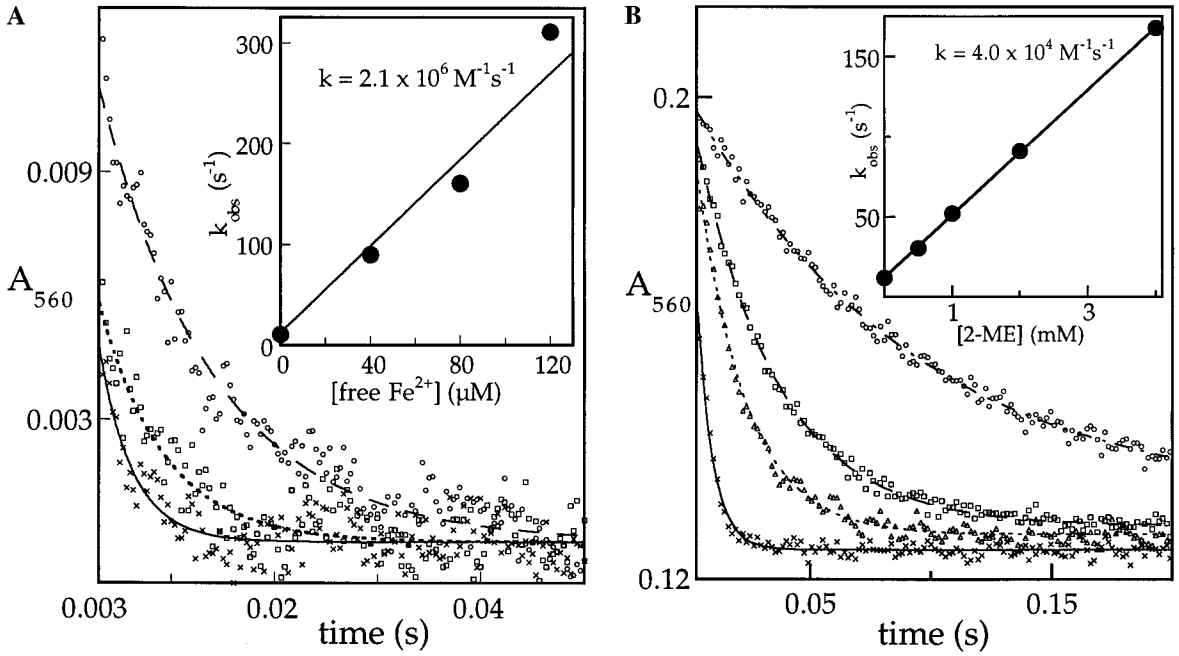

Figure 2. Reactivity of the 560-nm absorbing species toward the reductants, (A) $Fe(II)_{aq}$ and (B) 2-mercaptoethanol, as demonstrated by sequential-mixing stopped-flow absorption measurements. Apo R2 was mixed in the absence of O_2 with 2.3 equiv of Fe(II) prior to loading into the stopped-flow. This solution was mixed in the stopped-flow apparatus at 5 °C with an equal volume of O_2-saturated 100 mM Hepes buffer, pH 7.6, and after a 16 ms aging time, the resulting solution was mixed with 0.5 equiv volume of an O_2-free solution of either Fe(II) or 2-mercaptoethanol immediately prior to data acquisition. For part A, the final reactant concentrations were 0.020 mM R2 and either 0.04 mM *additional* Fe(II) delivered in the second mix (circular data points and dashed fit), 0.08 mM additional Fe(II) (square data points and dotted fit), or 0.12 mM additional Fe(II) (× points and solid fit). For part B, the final concentrations were 0.18 mM R2 (2.3 equiv Fe) and either 0 mM 2-mercaptoethanol (circular points and dash−dotted fit), 0.5 mM 2-mercaptoethanol (square points and dashed fit), 1 mM 2-mercaptoethanol (triangular points and dotted fit), or 4 mM 2-mercaptoethanol (× points and solid fit). In both A and B, the insets show plots of the observed first-order rate constants for decay (obtained by nonlinear regression fitting) versus concentrations of the reductants, from which second-order rate constants for reduction of the intermediate are derived.

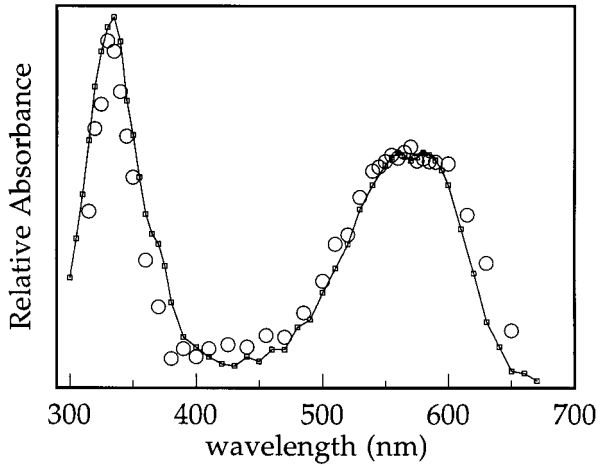

Figure 3. Kinetically resolved optical absorption spectrum of the 560-nm absorbing intermediate in the R2 reaction (circular points) and comparison to the published spectrum of the tryptophan cation radical (square points and solid interpolation fit) produced by pulse radiolysis of acidic aqueous tryptophan.[52] The experiment is described in the text. Each data point of the experimental spectrum represents the average amplitude of decay from 4 to 14 ms observed in three independent experiments after mixing the preformed intermediate with 2-mercaptoethanol at 5 °C. The final reactant concentrations were 0.18−0.19 mM R2 (2.3 equiv of Fe(II)) and 4 mM 2-mercaptoethanol.

of three samples for each reaction time exhibit an average of 34% (19 ms) and 31% (27 ms) greater integrated intensity than the spectra of product samples from the same reaction (Figure 4, spectrum D), which have 1.16 ± 0.04 equiv of tyrosyl radical. Thus, the Mössbauer and EPR data together imply that 1.55 ± 0.15 equiv of "spin" develops rapidly upon oxidation of 2.2 ± 0.2 equiv of Fe(II), and that only 1.0 ± 0.1 equiv of this spin can be attributed to **X**. The significant excess of spin equiv relative to **X** and the difference in line shape between the rapidly developing EPR signal and that of **X** indicate that a second EPR-active species (the $W^{+\bullet}$) forms along with **X**. In addition, analysis of the Mössbauer spectra (presented below) shows that, of the 1.0 equiv of **X** trapped in these early time points, approximately 0.6 equiv is magnetically coupled to a nearby Mössbauer-silent paramagnetic center. This analysis implies that a total of 1.60 equiv of spin should be detectable in the $g = 2$ region, which agrees well with the EPR spin quantitation.

As noted above, the Mössbauer spectrum at 4.2 K of the 19-ms sample exhibits the paramagnetic features characteristic of **X** (Figure 5). Component analysis of the spectrum acquired with a weak (50 mT) applied field (spectrum A) would suggest that 47 ± 5% of the total iron absorption is attributable to **X** (solid line plotted over the data), which would correspond to a stoichiometry of 0.7 ± 0.1 equiv of **X**. However, the spectrum of the same sample acquired with a strong (8 T) applied magnetic field (Figure 5, spectrum B) shows that 67 ± 5% of the total iron absorption (1.0 ± 0.1 equiv) can be assigned to **X** (solid line). As described in the accompanying paper,[62] an apparent discrepancy between the weak- and strong-field Mössbauer spectra in terms of the absorption intensity that is attributable to magnetically isolated **X** indicates that **X** is weakly spin-coupled to a nearby paramagnet. Since the EPR spectrum in the $g = 2$ region reflects more spin than **X**, this additional

(62) Krebs, C.; Chen, S.; Baldwin, J.; Ley, B. A.; Edmondson, D. E.; Huynh, B. H.; Bollinger, J. M., Jr. *J. Am. Chem. Soc.* **2000**, *122*, 12207−12219.

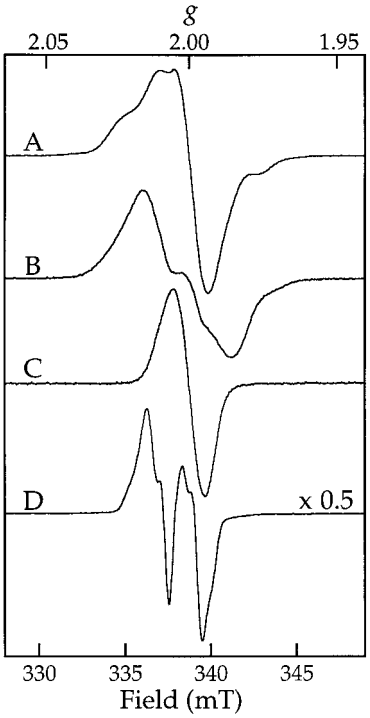

Figure 4. X-band EPR spectra at 20 K of 19 ms freeze-quenched samples from the reaction at 5 °C of O_2 with the Fe(II)-R2 complex (3.0 equiv of Fe) prepared either (A) with ^{56}Fe or (**B**) with ^{57}Fe. The final reactant concentrations were 1.3 mM O_2 and 0.47 mM R2. The spectrometer conditions for data acquisition were the following: microwave frequency, 9.48 GHz; microwave power, 6.3 μW, modulation frequency, 100 kHz; modulation amplitude, 4 G; scan time, 164 s; time constant, 164 ms. Spectrum C is a reference spectrum for **X** acquired on a sample that was prepared by mixing apo R2-Y122F at 5 °C in the presence of O_2 with excess ^{56}Fe(II) and freeze-quenching after 0.45 s. It has been shown that **X** is the only $g = 2.0$ EPR-active species that forms in this variant protein at short times under these reaction conditions[24,25,40] and that **X** in R2-Y122F is effectively indistinguishable from **X** in the wild-type protein.[40−42,44,45,75] The spectrometer frequency was 9.66 GHz for this spectrum. Its magnetic field axis has been mathematically corrected to correspond to a microwave frequency of 9.48 GHz to permit comparison to spectra A, B, and D. All other spectrometer conditions for spectrum C were identical with those for spectra A and B. Spectrum D is of the Y122•-containing, native R2 product of the reaction in part A. This sample was prepared by allowing the reaction to proceed for 3 min prior to freeze-quenching. The spectrometer conditions for spectrum D were the same as those for spectra A and B.

paramagnet (presumably the $W^{+\bullet}$) is assumed to have a spin (S) of $^1/_2$. Coupling between these adjacent $S = {}^1/_2$ species leads to a singlet $S = 0$ and a triplet $S = 1$ electronic state for the coupled system. Because the diiron center and W48 are separated by a distance of ∼10.8 Å (average distance in the structure of the oxidized protein from the atoms of the indole moiety expected to have significant spin density[63,64] to the center of the cluster[14]) the coupling between **X** and the $W^{+\bullet}$ is expected to be weak ($J < 1$ cm^{-1}). With such a weak coupling and in the presence of a weak (50 mT) applied field, the energy separations between these electronic levels will be small. At 4.2 K, all the levels should be almost equally populated. The singlet state and the $M_S = 0$ sublevel (which has a spin expectation value of zero) of the triplet state give rise to a Mössbauer spectral component consisting of quadrupole doublets, while the other two sublevels ($M_S = \pm 1$) of the triplet state yield a paramagnetic component identical with that of uncoupled **X**. Application of a strong magnetic field (e.g. 8 T), however, increases the energy separations between these levels due to the Zeeman effect and, at 4.2 K, depopulates all but the ground sublevel ($M_S = -1$). This effect renders the spectrum of **X** in the **X**-$W^{+\bullet}$ species indistinguishable from that of uncoupled **X** (see the following paper[62] for a more detailed explanation of this phenomenon). The observed difference of 20% in the intensities of the paramagnetic components in the weak- and strong-field spectra suggests that 40% of the total iron absorption is contributed by the **X**-$W^{+\bullet}$ species (i.e., 0.6 ± 0.1 equiv). This leaves 27% contribution from the uncoupled **X** (0.4 equiv).

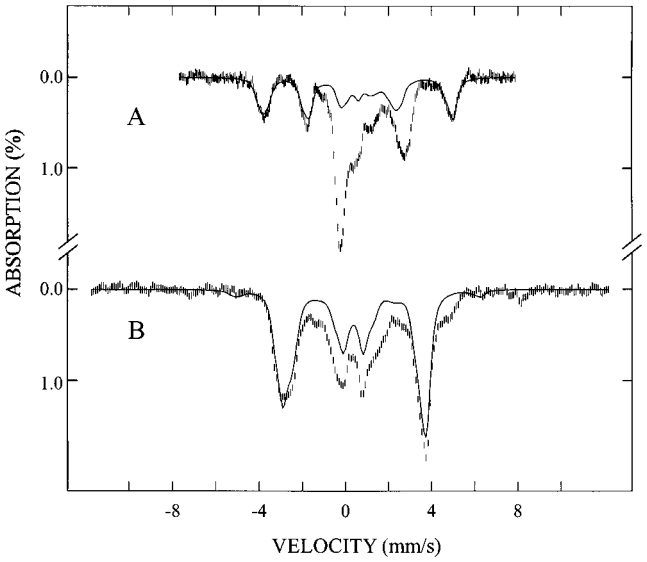

Figure 5. Mössbauer spectra at 4.2 K of a 19 ms freeze-quenched sample from the reaction at 5 °C of the Fe(II)-R2 complex (3.0 equiv of Fe) with O_2. The spectra were acquired with a magnetic field of either (A) 50 mT or (B) 8 T applied parallel to the γ-beam. The solid lines plotted over the data in parts A and B are theoretical spectra for **X**[43] plotted at intensities of 47% and 67%, respectively, of the total iron absorption area. The reactant concentrations were the same as those for spectrum B in Figure 4.

A graphic illustration and more quantitative analysis of the effects of spin coupling may be obtained from the spectra of the putative **X**-$W^{+\bullet}$ species at various applied fields after removal of the contributions of the unreacted Fe(II) (26%) and uncoupled **X** (27%) from the raw data (Figure 6). In a weak applied field (50 mT), the spectrum (spectrum A) displays substantial absorption in the central region resulting from the populated singlet state and $M_S = 0$ sublevel of the triplet state. As the field strength is increased (spectra B−E), the central absorption decreases due to the aforementioned Zeeman-induced depopulation of these two levels. Analysis of these spectra by iterative simulation according to eq 4 of the accompanying paper[62] and with parameters of **X** determined previously[43] indicates a spin coupling strength, J, on the order of 10^{-2}−10^{-1} cm^{-1}. The theoretical spectra shown, which correspond to $J = 0.05$ cm^{-1}, properly replicate the field dependence of the experimental spectra. (Note that the weak absorption peaks at −7 and at 8 mm/s, which contribute 4% of the total iron absorption, are attributed to the high-spin mononuclear $Fe(III)_{aq}$ species.) A requirement for the observed spin−spin interaction is close proximity of the two paramagnets. Thus, observation of spin-coupling effects in the Mössbauer spectra of **X** in the

(63) Krauss, M.; Garmer, D. R. *J. Phys. Chem.* **1993**, *97*, 831−836.
(64) Jensen, G. M.; Goodin, D. B.; Bunte, S. W. *J. Phys. Chem.* **1996**, *100*, 954−959.

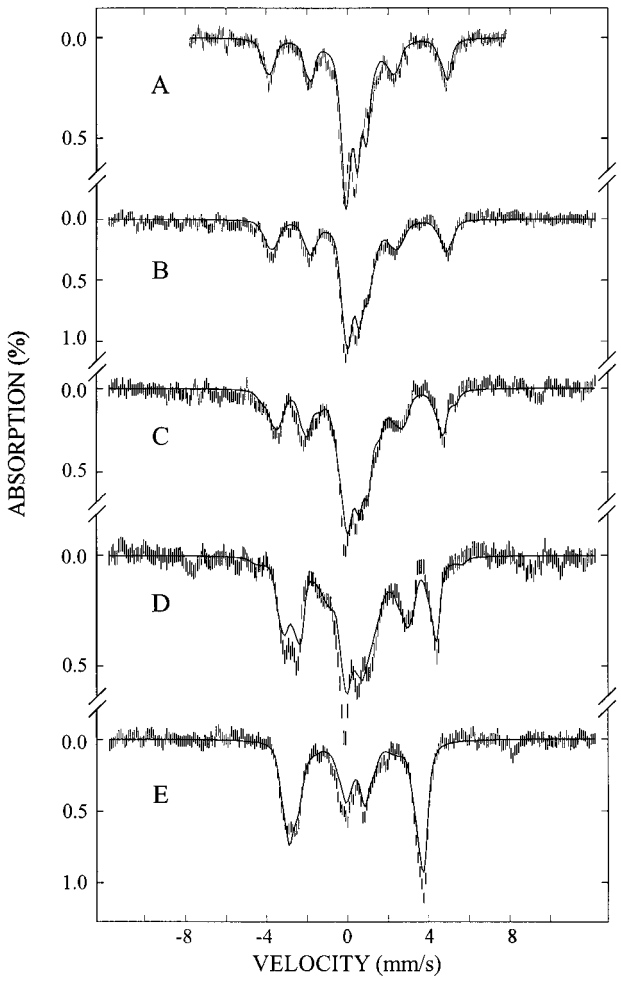

Figure 6. Field-dependent Mössbauer spectra of the **X**-$W^{+\bullet}$ diradical species acquired at 4.2 K with a magnetic field of (A) 50 mT, (B) 1 T, (C) 2 T, (D) 4 T, or (E) 8 T applied parallel to the γ-beam. In each case, the data were generated by subtracting the 26% contribution from unreacted Fe(II) and the 27% contribution from magnetically isolated **X** from the experimental spectrum of the sample of Figure 5 at that magnetic field. The theoretical spectra (solid lines plotted over the data) were generated according to the spin Hamiltonian (eq 4) given in the following paper,[62] with parameters for **X** determined previously[43] and $J = 0.05$ cm^{-1}.

19-ms sample provides compelling evidence that an additional radical forms along with **X**.

The measured Fe(II):spin stoichiometry is also evidence for the concomitant formation of **X** and the $W^{+\bullet}$. Whereas formation of **X** alone would require the oxidation of 3 equiv of Fe(II), with 2 equiv being incorporated into **X** and one being oxidized sacrificially to provide the extra electron, formation of each equivalent of the **X**-$W^{+\bullet}$ diradical species (having two equiv of spin) requires oxidation of only 2 equiv of Fe(II), yielding a limiting Fe(II):spin stoichiometry of 1. The observed stoichiometry of 1.4 (2.2 equiv of Fe(II) oxidized in production of 1.55−1.60 equiv of spin) mandates that a second radical species be produced along with **X** in a significant fraction of events. That this value is greater than the theoretical minimum of 1 is consistent with the deduction from the Mössbauer data that a significant quantity of uncoupled **X** forms along with the **X**-$W^{+\bullet}$ species. A portion of the former (0.12−0.18 equiv) can be explained to result from reduction of the $W^{\bullet+}$ by $Fe(II)_{aq}$, which also accounts for the high-spin Fe(III) species detected. The remainder of the uncoupled **X** (0.22−0.28 equiv) may reflect either inefficiency in freeze-trapping of the $W^{+\bullet}$ or the contribution of an alternative, minor mechanistic pathway for delivery of the extra electron that does not involve generation of the $W^{+\bullet}$.

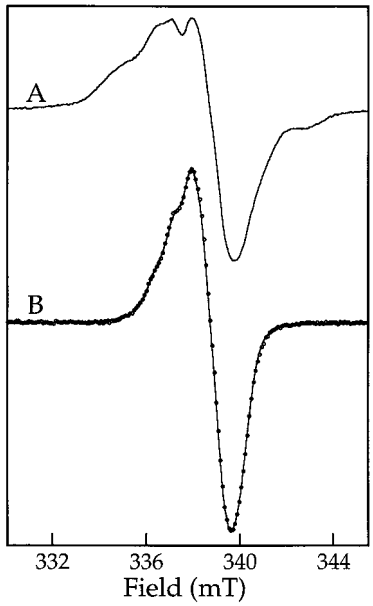

Figure 7. X-band EPR spectra at 20 K of freeze-quenched samples prepared by sequential mixing at 5 °C of the Fe(II)-R2 (3 equiv of Fe) complex with 2 vol equiv of O_2-saturated Hepes buffer and of the resulting solution with 0.67 vol equiv of either (A) O_2-free buffer or (B) O_2-free 3 mM $Fe(II)_{aq}$. The aging times were 17 ms between the first and second mixes and 8 ms between the second mix and freeze-quenching. The final protein concentration was 0.21 mM. The spectrometer conditions were the same as those given in the legend to Figure 4. In part B, the solid line is the experimental spectrum, and the circular points are a reconstruction of this spectrum prepared by summation of the reference spectra of **X** (Figure 4, spectrum C) and Y122$^{\bullet}$ (Figure 4, spectrum D) at relative intensities of 0.86:0.14.

On the basis of the above Mössbauer analysis, the EPR signal (Figure 4, A) may be understood as a superposition of two components arising from magnetically isolated **X** and spin-coupled **X**-$W^{+\bullet}$. The coupling of the two paramagnets in the diradical species is expected to broaden their EPR signals and, thus, to result in the broad, featured signal observed in the $g = 2$ region. To further test this explanation for the broad EPR signal, sequential-mixing freeze-quench EPR experiments were performed. The Fe(II)-R2 complex was mixed with O_2 and allowed to react for 17 ms to accumulate the **X**-$W^{+\bullet}$ intermediate, which was then reacted in the second mix with aqueous Fe(II) (1.2 mM *additional* Fe(II) after mixing, giving $t_{1/2} = 0.2$ ms for the putative $W^{+\bullet}$) or 2-mercaptoethanol (16 mM after mixing, giving $t_{1/2} = 1$ ms) for 8 ms prior to freeze-quenching. For each experiment, a control sample was prepared in which the second mix was with buffer, which allows the intermediate species to decay more slowly with its intrinsic rate constant of $\sim$12 s^{-1} and therefore to be freeze-trapped after the 8 ms second incubation. Reacting the intermediate with either 2-mercaptoethanol (data not shown) or additional Fe(II) (Figure 7, spectrum B, solid line) results in disappearance of the broad features and significant loss of $g = 2$ EPR intensity (30−32% decrease in six trials with 2-mercaptoethanol; 40 and 42% in two trials with Fe(II)[65]) relative to the buffer control (Figure 7, spectrum A). After mixing with additional Fe(II), the spectrum that remains

(65) The fact that the loss of intensity upon reaction with 2-ME is somewhat less than upon reaction with $Fe(II)_{aq}$ is attributable to freeze-trapping of a small quantity of some sort of 2-ME radical, which is observable in the EPR spectrum of these samples.

can be reconstructed by summing reference spectra for **X** and Y122• at relative intensities of 0.86:0.14 (circular points plotted over the experimental spectrum). The integrated intensity of this spectrum corresponds to 1.0 equiv of spin (1.02 and 1.00 equiv in two trials), which implies that 0.86 equiv of **X** remains after 8 ms of reaction with additional Fe(II). This value is similar to the 1.0 ± 0.1 equiv determined by Mössbauer analysis of the single-mix samples that were freeze-quenched at similar (slightly shorter) reaction times, confirming that **X** does not react rapidly (relative to the 8 ms second aging time) with 1.2 mM $Fe(II)_{aq}$. The integrated intensity of the spectrum of the control sample in which the second mix was with buffer reflects 1.7 equiv of spin (1.67 and 1.69 in two trials), which is within the range observed in the single-mix experiments and again is much more than can possibly be attributed to **X**. Thus, mixing the preformed intermediate with reductant, which is known to lead to rapid decay of the 560-nm-absorbing component, is also associated with loss of the broad $g = 2.0$ EPR features and a decrease in total EPR intensity that cannot be explained by decay of **X**. This correlation is strong evidence that the absorbing species is a radical. The Fe(II) experiment is especially compelling evidence for accumulation of a diradical species in the first mix, in view of the fact that Fe(II) delivered in the second mix could, in principle, support development of *more* $g = 2$ intensity in the form of additional **X** and/or Y122•, but instead results in a *loss* of intensity corresponding to ~0.7 equiv.

The combined chemical, optical, EPR, and Mössbauer characterization of the 560-nm-absorbing species provides strong evidence for the $W^{+\bullet}$ assignment: its absorption spectrum is nearly an exact match with the very distinctive published spectrum of $W^{+\bullet}$ generated by pulse radiolysis of acidic aqueous tryptophan and Trp containing peptides;[52,53] it is associated with EPR absorption in the $g = 2.0$ region and perturbs the EPR and Mössbauer spectra of **X**; and it reacts rapidly with three different reductants. In the following paper, we demonstrate that substitution of W48 with F eliminates the reductant-sensitive 560-nm absorption and disables rapid injection of the extra electron.[62] When considered with the structural similarity of the H-bond networks involving W48 in R2[13,14] and W191 in yeast cytochrome C peroxidase[54] and the fact that a $W191^{+\bullet}$ forms in the latter upon heterolytic cleavage of a peroxide substrate bound to the enzyme's heme Fe center,[55,57,58] these data leave little room for doubt that the $W^{+\bullet}$ assignment is correct and that W48 is the site of the radical.

Determination of the Concentration of $Fe(II)_{aq}$ in the Fe(II)-R2 Reactant Solution. Concomitant formation of **X** and $W^{+\bullet}$ should yield a quantity of spin nearly twice that of **X**. The fact that the quantity of spin successfully trapped is somewhat less than twice the quantity of **X** can be partly accounted for by the rapid reduction of some $W^{+\bullet}$ by free Fe(II). This "side reaction" reduces the total concentration of $g = 2.0$ EPR active species, increases the quantity of Fe(II) oxidized (to increase the observed Fe(II):spin stoichiometry above the theoretical value of 1), and presumably produces the high-spin Fe(III) species observed by Mössbauer. The concentration of free Fe(II) under these conditions was determined directly in a stopped-flow experiment in which the Fe(II)-R2 reactant solution (same concentrations as in Figures 4 and 5) was mixed at 5 °C in the absence of O_2 with the colorimetic Fe(II) indicator, ferrozine (5 mM final concentration). Under the conditions of this mix, free Fe(II) is converted to the colored complex with an effective rate constant of 120 ± 10 s^{-1} (as shown by control experiments in which $Fe(II)_{aq}$ was mixed with ferrozine under the same conditions) while bound Fe(II) undergoes chelation quite slowly

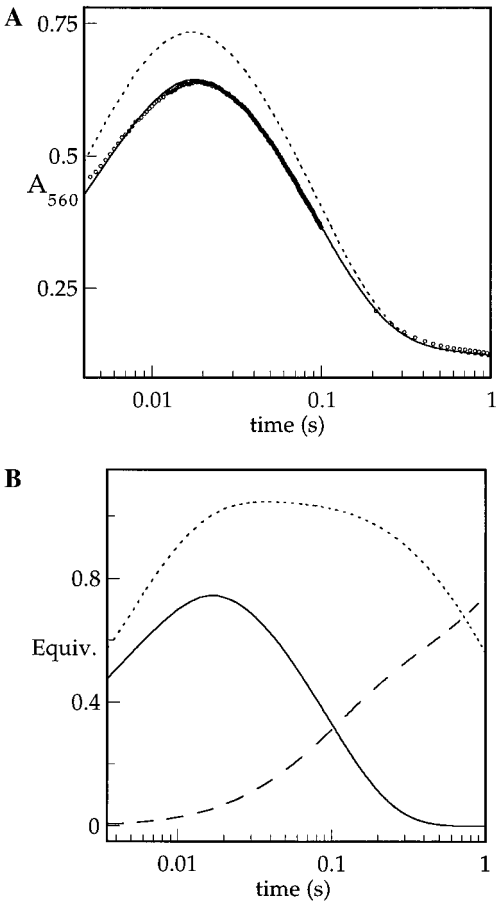

Figure 8. Comparison of the timecourse of absorbance at 560 nm for the reaction at 5 °C of the Fe(II)-R2 complex (3.0 equiv of Fe) with O_2 to that predicted by Scheme 1 and the kinetic and spectral parameters given in Tables 1 and 2. (A) Experimental timecourse of absorbance at 560 nm (circular points) from the reaction described in the legend to Figure 4B compared to that predicted by assuming *no* free Fe(II) (dotted line) and to that predicted by assuming 0.17 equiv (0.073 mM) of free Fe(II) (solid line). (B) Simulated timecourses of $W^{+\bullet}$ (solid line), **X** (dotted line), and Y122• (dashed line) under the same reaction conditions. The precise values of reactant concentrations and kinetic parameters used in this simulation may be found in Table 2.

($k < 0.1$ s^{-1}, as revealed by experiments in which Fe(II)-R2 with low Fe(II)/R2 ratios was mixed with ferrozine under the same conditions), presumably because of its slow dissociation from the protein. The amplitude of the rapid chelation phase observed in these experiments corresponds to 0.2 ± 0.04 equiv of unbound Fe(II), which is within experimental uncertainty of the quantity of high-spin Fe(III) determined from analysis of the Mössbauer spectra (0.12 ± 0.06 equiv). Consistent with these measurements, the A_{560}-versus-time trace from the reaction can be successfully simulated (according to Scheme 1 and with the quantity of **X** that is known from the Mössbauer experiments constraining the value of the initial concentration of reactive Fe(II)-R2 complex) if the presence of 0.17 equiv of free Fe(II) is assumed (Figure 8A, solid line). By contrast, too large an amplitude is predicted if the $[Fe(II)_{aq}]$ is assumed to be zero (Figure 8A, dotted line). The better simulation of Figure 8A predicts that, between 19 and 27 ms, the quantities of **X** (Figure 8B, dotted line), $W^{+\bullet}$ (solid line), and Y122• (dashed line) vary from 1.02 to 1.04 equiv, from 0.74 to 0.71 equiv, and from 0.07 to 0.1 equiv, respectively, while the total quantity of spin remains almost constant at approximately 1.8 equiv. We consider the difference between the measured and theoretical quantities

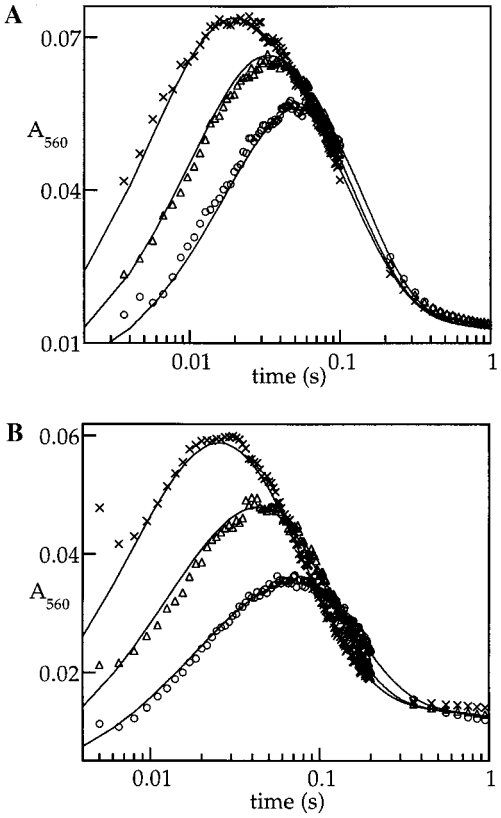

Figure 9. First-order dependencies of the rate of formation of the 560-nm-absorbing intermediate at 5 °C on the concentrations of (A) O_2 and (B) Fe(II)-R2 complex. In part A, the reactant concentrations were 0.09 mM R2 (2.3 equiv Fe) and either 0.21 mM O_2 (circular points), 0.42 mM O_2 (triangular points), or 0.83 mM O_2 (× points). In part B, the reactant concentrations were 0.051 mM O_2 and either 0.17 mM R2 (circular points), 0.35 mM R2 (triangular points), or 0.69 mM R2 (× points), with 2.7 equiv of Fe(II) in each case. The solid lines plotted over the data are simulations according to Scheme 1 and the parameters given in Table 2.

of total spin (1.6−1.7 equiv compared to 1.8 equiv) to be less than the experimental uncertainty associated with the measurements.

Concentration Dependencies of the Kinetics of $W^{+\bullet}$ Formation. The dependencies of the rate of $W^{+\bullet}$ formation on O_2 and Fe(II)-R2 concentrations were examined in a series of stopped-flow experiments in which absorbance at 560 nm was monitored. In one set of trials, the concentration of O_2 was varied at a fixed concentration of Fe(II)-R2 complex (with O_2 maintained in excess), and in a second, the concentration of Fe(II)-R2 complex was varied at a fixed concentration of O_2 (with Fe(II)-R2 maintained in excess). A representative set of traces from the varied [O_2] experiments (Figure 9A) shows that $W^{+\bullet}$ formation is first order in O_2. The traces can be simulated well according to kinetic Scheme 1 (solid lines plotted over data), in which formation of the $W^{+\bullet}$ species results from a bimolecular reaction between the Fe(II)-R2 complex and O_2, with no accumulation of intervening intermediates. Traces from the varied [Fe(II)-R2] experiments (Figure 9B) also reflect strictly second-order kinetics, and can be simulated according to Scheme 1 (solid lines). These kinetics require that intermediates between the reactants and the **X**-$W^{+\bullet}$ species in Scheme 1 must decay to the diradical species rapidly with respect to their formation. For example, the peroxodiiron(III) complex proposed to be a precursor[27] would have to decay with a rate constant of at least ~400 s^{-1} for the simulated A_{560}-versus-time traces not to disagree egregiously with the stopped-flow traces. This

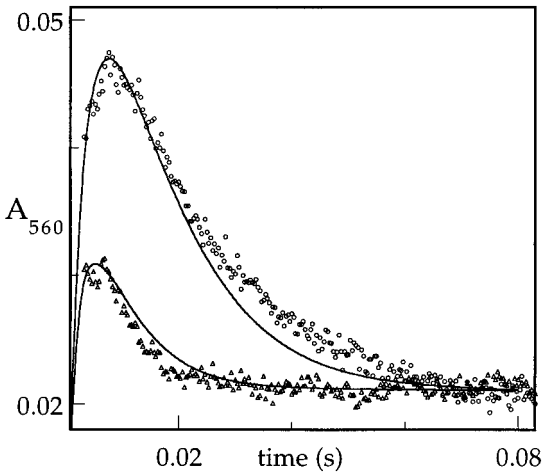

Figure 10. Suppression of the transient absorbance at 560 nm at high Fe(II)/R2 ratios. R2 that had been premixed with either 5 equiv of Fe(II) (circular points) or 8 equiv of Fe(II) (triangular points) was mixed at 5 °C in the stopped-flow apparatus with 2 vol equiv of O_2-saturated Hepes buffer. The final protein concentration was 0.058 mM. The solid lines plotted over the data are simulations according to Scheme 1 and the parameters given in Table 2.

observation is of interest because, of the peroxodiiron(III) complexes detected in the similar O_2 reactions mediated by MMOH,[32−35,37] Δ9D,[66,67] the D84E variant of *E. coli* R2,[30,68] and the ferrooxidase site of ferritin,[69−71] the ferritin intermediate decays most rapidly at 4 s^{-1} at 22 °C. Accounting for the difference in reaction temperature, the ferritin complex decays perhaps 400-fold less rapidly than the lower limit set for decay of the possible peroxodiiron(III) complex in wildtype *E. coli* R2. Thus, either the R2 protein "tunes" this intermediate complex to be much more reactive than the cognate species in the other proteins or the R2 reaction proceeds through a different, more reactive diiron(II)-O_2 complex. The available data provide no compelling reason to exclude either possibility. Answering this question should require a method to allow accumulation of the precursor(s) to the **X**-$W^{+\bullet}$ species. One obvious possible approach, which is explored in the following paper,[62] is mutagenesis of W48 to disable the rapid reduction of the precursor complex.

Evidence for Intermediacy of the $W^{+\bullet}$ also with Excess Fe(II). The second-order rate constants for reaction of the Fe(II)-R2 complex with O_2 and for reduction of the $W^{+\bullet}$ by free Fe(II) determined in this study ($(2.2 \pm 0.3) \times 10^5$ M^{-1} s^{-1} and $(2.1 \pm 0.5) \times 10^6$ M^{-1} s^{-1}, respectively) allow the prediction that the $W^{+\bullet}$ should accumulate significantly at typical reactant concentrations (e.g. ~800 μM O_2, ~100 μM R2), even with an Fe(II)/R2 ratio as high as 5.0. Confirming this prediction, the 560-nm transient absorption is not completely suppressed at this ratio (Figure 10, circular points) and a further increase to Fe(II)/R2 = 8.0 (triangular points) is associated with further reduction in the transient amplitude. These A_{560}-versus-time

(66) Broadwater, J. A.; Ai, J.; Loehr, T. M.; Sanders-Loehr, J.; Fox, B. G. *Biochemistry* **1998**, *37*, 14664−14671.
(67) Broadwater, J. A.; Achim, C.; Münck, E.; Fox, B. G. *Biochemistry* **1999**, *38*, 12197−12204.
(68) Moënne-Loccoz, P.; Baldwin, J.; Ley, B. A.; Loehr, T. M.; Bollinger, J. M., Jr. *Biochemistry* **1998**, *37*, 14659−14663.
(69) Pereira, A. S.; Small, W.; Krebs, C.; Tavares, P.; Edmondson, D. E.; Theil, E. C.; Huynh, B. H. *Biochemistry* **1998**, *37*, 9871−9876.
(70) Moënne-Loccoz, P.; Krebs, C.; Herlihy, K.; Edmondson, D. E.; Theil, E. C.; Huynh, B. H.; Loehr, T. M. *Biochemistry* **1999**, *38*, 5290−5295.
(71) Huang, J.; Krebs, C.; Huynh, B. H.; Edmondson, D. E.; Theil, E. C.; Penner-Hahn, J. E. *Science* **2000**, *287*, 122−125.

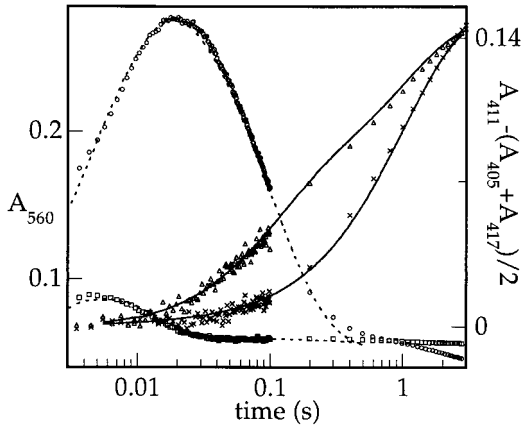

Figure 11. Dependencies of the timecourses of absorbance at 560 nm and Y122• formation on the ratio Fe(II)/R2. The A_{560}-versus-time traces from Figure 1 for 3.2 equiv of Fe (circular points) and 6.0 equiv of Fe (square points) are replotted for comparison with traces simulated according to Scheme 1 and the parameters given in Table 2 (dotted traces). The corresponding timecourses of Y122• formation (as reflected by the 411 nm peak height) for the same reactions are also shown (triangular points for 3.2 equiv of Fe and x points for 6.0 equiv of Fe) and compared to traces from the same simulations (solid lines). The reactant concentrations are given in the legend to Figure 1.

traces can be simulated according to Scheme 1 (solid lines over data), but the simplest assumption that any Fe(II) in excess of 3.2 equiv remains unbound and available to reduce the $W^{+\bullet}$ with the measured second-order rate constant leads to a slight *under*prediction of the transient amplitude for Fe(II)/R2 = 8. The data suggest that the protein is capable of binding up to 4.0 equiv of Fe(II), as the assumption of 4 equiv of free Fe(II) in the Fe(II)/R2 = 8 experiment of Figure 10 leads to accurate simulation of the A_{560} kinetics according to Scheme 1. It is likely that the protein is heterogeneous and that 20% of the diiron cluster sites bind Fe(II) less tightly and unproductively for both rapid production of intermediates and tyrosyl radical formation. Indeed, heterogeneity in reactivity toward both O_2 and electrochemical reduction has been observed previously,[31] and our results may simply be another manifestation of this. The relevant point is that the transient absorption persists as Fe(II)/R2 becomes sufficiently high that all reasonably tight-binding sites should be occupied, and its suppression is related to the concentration of *free* Fe(II). These observations are consistent with the hypotheses that (1) the $W^{+\bullet}$ is an intermediate also in the excess Fe(II) reaction and (2) the mechanisms of the limiting and excess Fe(II) reactions diverge according to the fate of this common intermediate rather than in the identity of an earlier intermediate.

Fate of the $W^{+\bullet}$ with Limiting Reductant. Scheme 1 predicts that, in the absence of a reductant to provide the extra electron, some Y122• should be produced by the $W^{+\bullet}$ (in the step associated with k_4) and this Y122• should form faster than that produced by **X** in the k_5-associated step. Indeed, the faster production of Y122• in reaction of the apo protein with limiting Fe(II) than in its reaction with excess Fe(II) or with limiting Fe(II) in the presence of ascorbate was previously demonstrated.[26] This kinetic difference is also observed when the Fe(II)-R2 complex is formed prior to its exposure to O_2 (Figure 11; compare triangular points for Fe(II)/R2 = 3.2 with × points for Fe(II)/R2 = 6.0). With Fe(II)/R2 = 3.2, Y122• formation is biphasic after the lag phase associated with accumulation of the diradical species. This complexity is accounted for in Scheme 1 by formation of Y122• in two distinct steps: the faster, k_4-associated step, in which the $W^{+\bullet}$ generates the Y122•, and the slower k_5-associated step, in which **X** generates the Y122• after the $W^{+\bullet}$ has been reduced by an exogenous source. A portion of the slower phase can be explained by the presence of some free Fe(II), which rapidly reduces a fraction of the $W^{+\bullet}$ (in the k_2-associated step). However, simulation of the A_{560}-versus-time trace from the same reaction indicates that the concentration of free Fe(II) cannot be sufficient to account for all the Y122• produced in the slow phase. This observation requires the existence of the k_3-associated pathway, in which the exogenous electron is provided by some source other than $Fe(II)_{aq}$. The dependencies of the kinetics of decay of the $W^{+\bullet}$ on pH and on the concentration and pK_a of the buffer indicate that the basic form of a piperazine- or morpholine-based buffer (such as HEPES, which was employed in this study) may serve as the electron source (J. Baldwin, B. Ley, J. Bollinger, unpublished data). The timecourses of Y122• formation with Fe(II)/R2 = 3.2 and Fe(II)/R2 = 6.0 can both be simulated well according to Scheme 1 (solid lines plotted over the data) by using parameters that also account well for the timecourses of A_{560} for the same reactions (dotted lines).

As noted in our previous work, the generation of Y122• by the $W^{+\bullet}$ of the **X**-$W^{+\bullet}$ species should produce an intermediate containing both **X** and Y122•.[26] R2-W48F, which is the subject of the following article,[62] accumulates nearly a stoichiometric quantity of this diradical species upon O_2 activation and has allowed its spectroscopic characteristics to be determined. As a result of spin-coupling between its two adjacent radical components, it exhibits a very broad, featured $g = 2.0$ EPR signal (Figure 12A, circular data points), which is very different from the sum of the spectra of the two radicals in isolation. The spectrum of the 0.34 s timepoint from the reaction of the wild-type Fe(II)-R2 complex (3 equiv Fe) with 1.3 mM O_2 (Figure 12A, solid line) clearly exhibits the same broad EPR features as the **X**-Y• species from R2-W48F. These features are broader than those of the initial **X**-$W^{+\bullet}$ diradical species (Figure 12A, dotted line), and account for 46% of the integrated intensity of the 0.34-s time-point spectrum. The full experimental spectrum (Figure 12B, solid line) can be reconstructed by adding the spectra of the **X**-Y• species, uncoupled **X** and uncoupled Y122• at relative intensities of 0.46:0.37:0.17 (Figure 12B, dotted line). This reconstruction and the integrated intensity of the experimental spectrum imply that 0.36 equiv of the X-Y• species, 0.58 equiv of uncoupled **X**, and 0.26 equiv of uncoupled Y122• are present in the 0.34 s sample. By comparison, the simulation of Figure 8 predicts that 0.38 equiv of the **X**-Y• species, 0.48 equiv of uncoupled **X**, and 0.18 equiv of uncoupled Y122• should be present at 0.34 s. We consider the agreement among these values to be very good. More importantly, the qualitative observation of the EPR signature of the **X**-Y• diradical species proves that an additional species besides **X** (the $W^{+\bullet}$) can generate Y122•.[72]

In summary, all of the kinetic and spectroscopic data presented herein are consistent with the previously proposed mechanism for transfer of the extra electron, in which W48 is transiently oxidized to a $W^{+\bullet}$ and then reduced by $Fe(II)_{aq}$, ascorbate, or 2-mercaptoethanol. The conclusion that this residue is initially oxidized in preference to Y122 is perhaps surprising, since the latter is spatially closer to the diiron cluster (in the structure of the diiron(III) protein it is 5.3 Å from the phenolic O of Y122 to Fe1 compared to 8.8 Å from the indole N of W48 to Fe1[14]) and is expected to be a better reductant thermodynamically.[73,74] Moreover, the reactivities of W48 and

(72) We note that the generation of tyrosyl radicals by W cation radicals is well-precedented by studies of Klapper and co-workers (e.g. ref 74).

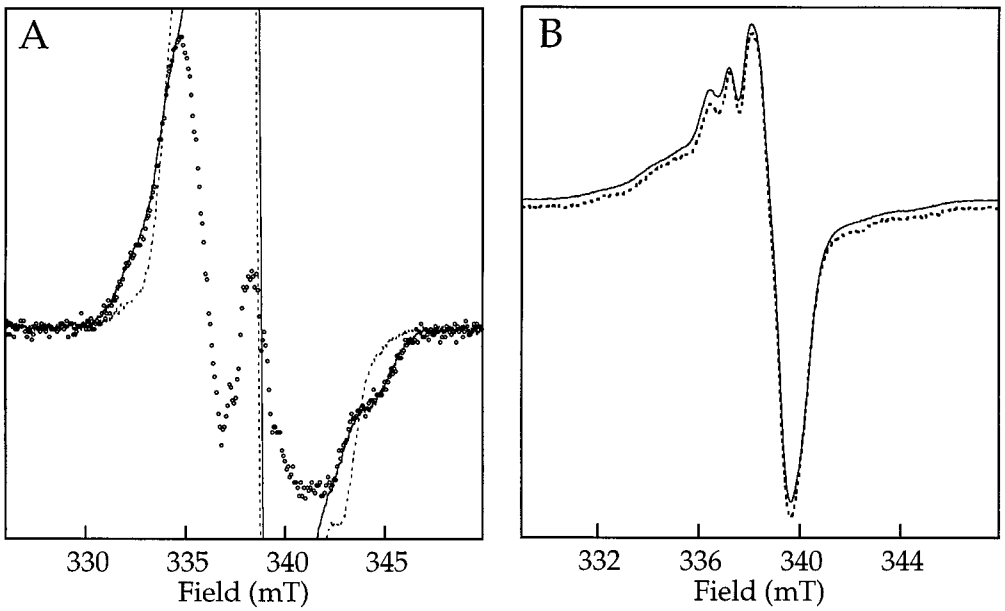

Figure 12. Quantitative analysis of the 20 K X-band EPR spectrum from a reaction sample that was freeze-quenched (at 0.34 s) after decay of the $W^{+\bullet}$: (A) detection of the broad signature of the **X**-Y$^\bullet$ species and (B) account of the spectrum by summation of the spectra of X-Y$^\bullet$, **X** and Y122$^\bullet$. In part A, the solid line is the experimental spectrum of the 0.34 s sample, and the open circles are an experimental reference spectrum of the **X**-Y$^\bullet$ species prepared (as described in the following paper[62]) from the spectrum of a freeze-quenched (1.4 s) sample from the reaction at 5 °C of apo R2-W48F with Fe(II) (2.5 equiv) and O_2 (1 mM). The latter is plotted at an intensity corresponding to 46% of the former. The dotted line is the spectrum of the 19 ms sample from the wild-type R2 reaction (Figure 4, spectrum A) shown for comparison. In part B, the solid line is the experimental spectrum in part A, and the dotted line was constructed by summation of the reference spectra of X-Y$^\bullet$, **X** (Figure 4, spectrum C) and Y122$^\bullet$ (Figure 4, spectrum D) at relative intensities of 0.46:0.37:0.17. With the exception of the reaction time, the 0.34 s sample was identical with the sample on which Figure 4, spectrum A was acquired. The spectrometer conditions were identical with those used to acquire that spectrum.

Y122 toward oxidation by cluster **X** are clearly reversed: **X** oxidizes Y122 in preference to W48. This reversal in the relative reactivity of the W48 and Y122 side chains is the essence of the electron gating that the R2 protein must exercise to split the two oxidizing equivalents of the initial complex between its diiron(II) cluster and O_2 and thereby to effect a one-electron-oxidation outcome. The structural, dynamical, and thermodynamical bases for this reversal remain to be elucidated.

(73) Jovanovic, S. V.; Steenken, S.; Simic, M. G. *J. Phys. Chem.* **1991**, *95*, 684−687.

(74) DeFelippis, M. R.; Murthy, C. P.; Broitman, F.; Weintraub, D.; Faraggi, M.; Klapper, M. H. *J. Phys. Chem.* **1991**, *95*, 3416−3419.

(75) Tong, W.; Burdi, D.; Riggs-Gelasco, P.; Chen, S.; Edmondson, D.; Huynh, B. H.; Stubbe, J.; Han, S.; Arvai, A.; Tainer, J. *Biochemistry* **1998**, *37*, 3840−3848.

Acknowledgment. This work was supported by NIH grants GM55365 (J.M.B) and GM47295 (B.H.H.) and by grants from the Searle Scholars Program of the Chicago Community Trust and the Camille and Henry Dreyfus Foundation (to J.M.B.).

Supporting Information Available: Details of the preparation of Fe(II)-R2 and freeze-quenched samples, description of EPR spectrometers used, procedures to determine molar absorptivities at 560 nm, and a discussion of the magnitude of uncertainties in various parameters used in the simulations (PDF). This material is available free of charge via the Internet at http://pubs.acs.org.

JA001278U